

Analytic solution of the gravity anomaly of irregular 2D masses with density contrast varying as a 2D polynomial function

Xiaobing Zhou¹

ABSTRACT

The analytic solution of the gravity anomaly caused by a 2D irregular mass body with the density contrast varying as a polynomial function in the horizontal and vertical directions is extrapolated from a historical version in which the analytic solution for the gravity anomaly was given only at the origin of the coordinate system to any point for the density function in terms of variables relative to that origin. To calculate the gravity anomaly at stations that are not at origins, a coordinate transformation is performed, in which case the polynomial density contrast function must also be expressed in the transformed coordinates, or a transformed solution must be obtained. These analytic solutions can be obtained at any station using (1) a solution transformation method, in which the density function and boundary of a mass body are kept intact, or (2) a coordinate transformation method, in which polynomial coefficient and boundary of a mass body are transformed accordingly. The issue of singularity and instability of the analytic methods has been related to case studies. Caution should be exercised in modeling or interpreting the gravity survey data using the analytic methods for large target-distance-to-target-size ratios outside the range of numerical stability. Compared with other published methods, the analytic solution results agree very well with other numerical or seminumerical methods, indicating the solution is correct and can be applied for any gravity anomaly calculation caused by an irregular 2D mass body with the density-contrast approximated as a polynomial function of horizontal position and/or vertical position when the observation is within the range of numerical stability.

INTRODUCTION

Gravity exploration requires high accuracy and speed in gravity forward modeling and inversion so that the gravity anomaly can be accurately modeled and subsurface geologic structure can be accu-

rately inverted from survey data. An analytic (also called closed-form) solution of the gravity anomaly caused by a specific mass body is often vigorously pursued. However, a closed-form solution is usually very difficult to find. In this article, I give an analytic solution at any point in space for a 2D polygon mass body with density contrast varying in a polynomial function of horizontal x , vertical z , or x and z , i.e.,

$$\sigma(x,z) = \sum_{i=0}^{N_x} \sum_{j=0}^{N_z} a_{i,j} x^i z^j, \quad (1)$$

where $\sigma(x,z)$ is the density contrast at source point (x,z) , constants a_{ij} are the coefficients of the polynomial, and N_x and N_z are the maximum power of x and z , respectively.

This problem has been studied by Zhang et al. (2001). Zhou (2009b) corrects some errors in Zhang et al.'s (2001) solution when the density model includes coordinate x and gives a complete set of equations that are programmable to provide the gravity anomaly at the origin. However, the closed-form solution in these studies is valid and useful for the gravity-anomaly calculation only at the origin. For the gravity-anomaly calculation at a station that is not at the origin, the formulation in these studies can be obtained through (1) a coordinate transformation (CT) to make the station the origin of the new coordinate system so the solution at origin can be directly used or (2) a solution transformation (ST), in which the solution at any point is obtained without transforming the coordinate system. To make the solution at the origin usable for any observation point in the option of coordinate transformation, the density contrast in the new coordinate must be expressed as a polynomial function, too. For a specific mass source model of defined density-contrast profile and the geometry, a coordinate transformation is performed for each station, resulting in a new density-contrast profile and geometry.

In the following discussion, the ST method is discussed first, followed by the CT method. For the ST method, the solution at origin is extrapolated to a solution at any point, keeping the density-contrast function and the geometry of the mass body intact. A complete set of analytic equations is thus obtained that can be programmed for calculating the gravity anomaly when the density contrast is a poly-

Manuscript received by the Editor 3 March 2009; revised manuscript received 29 September 2009; published online 12 March 2010.

¹Montana Tech of the University of Montana, Department of Geophysical Engineering, Butte, Montana, U.S.A. E-mail: xzhou@mtech.edu.
© 2010 Society of Exploration Geophysicists. All rights reserved.

mial function of both x and z , with cases in which the density contrast is a polynomial function in either direction as special cases. For the CT method, the polynomial coefficient of the density function and the geometry of the source body are transformed accordingly. The solution at origin (Zhou, 2009b) is expressed in the original coordinate system, so the forward modeling for a gravity survey can be automated using the survey coordinate system (original system). Singularity and numerical instability are then discussed, followed by algorithm validation using case studies and comparison for the analytic solutions by both methods. The following is based on Zhang et al. (2001) and Zhou (2009b), and most of the notations are the same as in those two articles.

ANALYTIC SOLUTION

I first discuss the analytic solution obtained by the ST method. Consider a geometry and coordinate system set up as in Figure 1. The gravity at any station $P(x_0, z_0)$ along the x -axis (equation 5 of Zhang et al., 2001) for the vertical component of a gravity anomaly caused by a 2D mass becomes

$$\Delta g_z(x_0, z_0) = 2G \sum_{i=0}^{N_x} \sum_{j=0}^{N_z} a_{i,j} \iint_S \frac{x^i z^j (z - z_0)}{(x - x_0)^2 + (z - z_0)^2} dx dz. \quad (2)$$

Consider the following identities:

$$\begin{aligned} & \frac{x^i z^j (z - z_0)}{(x - x_0)^2 + (z - z_0)^2} \\ &= \frac{[(x - x_0) + x_0]^i [(z - z_0) + z_0]^j (z - z_0)}{(x - x_0)^2 + (z - z_0)^2} \\ &= \sum_{m=0}^j C_j^m(z_0)^m \sum_{n=0}^i C_i^n(x_0)^n \frac{(x - x_0)^{i-n} (z - z_0)^{j-m+1}}{(x - x_0)^2 + (z - z_0)^2}, \end{aligned} \quad (3)$$

where C_i^n and C_j^m are the binomial expansion coefficients. An equation similar to equation 6 of Zhang et al. (2001) can be then obtained:

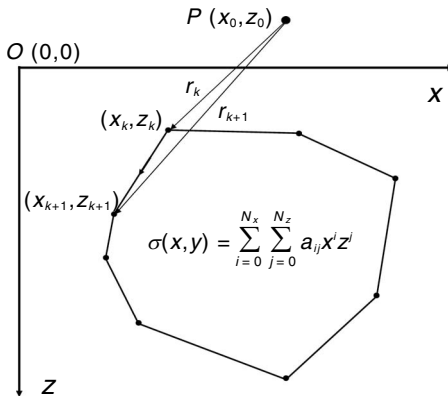


Figure 1. A schematic for the gravity anomaly at a general point $P(x_0, z_0)$ resulting from a 2D mass of polygon with density contrast in the form of a polynomial function of x and z .

$$\begin{aligned} & \frac{(x - x_0)^{i-n} (z - z_0)^{j-m+1}}{(x - x_0)^2 + (z - z_0)^2} = \frac{1}{i + j - m - n + 1} \\ & \times \left\{ \frac{\partial}{\partial x} \left[\frac{(x - x_0)^{i-n+1} (z - z_0)^{j-m+1}}{(x - x_0)^2 + (z - z_0)^2} \right] \right. \\ & \left. + \frac{\partial}{\partial z} \left[\frac{(x - x_0)^{i-n} (z - z_0)^{j-m+2}}{(x - x_0)^2 + (z - z_0)^2} \right] \right\}. \end{aligned} \quad (4)$$

Therefore,

$$\frac{x^i z^j (z - z_0)}{(x - x_0)^2 + (z - z_0)^2} = \frac{\partial A_x}{\partial z} - \frac{\partial A_z}{\partial x}, \quad (5)$$

where the 2D vector gravity potential \mathbf{A} takes the form (Zhou, 2008)

$$\begin{cases} A_x = \sum_{m=0}^j C_j^m(z_0)^m \sum_{n=0}^i C_i^n(x_0)^n \frac{1}{i + j - m - n + 1} \\ \quad \times \frac{(x - x_0)^{i-n} (z - z_0)^{j-m+2}}{(x - x_0)^2 + (z - z_0)^2} \\ A_z = - \sum_{m=0}^j C_j^m(z_0)^m \sum_{n=0}^i C_i^n(x_0)^n \frac{1}{i + j - m - n + 1} \\ \quad \times \frac{(x - x_0)^{i-n+1} (z - z_0)^{j-m+1}}{(x - x_0)^2 + (z - z_0)^2} \end{cases}. \quad (6)$$

Applying Stokes' theorem to equation 2,

$$\begin{aligned} & \iint_S \frac{x^i z^j (z - z_0)}{(x - x_0)^2 + (z - z_0)^2} dx dz \\ &= \iint_S \left(\frac{\partial A_x}{\partial z} - \frac{\partial A_z}{\partial x} \right) dx dz = \oint_C (A_x dx + A_z dz). \end{aligned} \quad (7)$$

The vertical component of a gravity anomaly at station $P(x_0, z_0)$ becomes

$$\begin{aligned} \Delta g_z(x_0, z_0) &= 2G \sum_{i=0}^{N_x} \sum_{j=0}^{N_z} a_{i,j} \sum_{m=0}^j C_j^m(z_0)^m \\ & \times \sum_{n=0}^i \frac{C_i^n(x_0)^n}{i + j - m - n + 1} \\ & \times \left(\oint_C \frac{(x - x_0)^{i-n} (z - z_0)^{j-m+2}}{(x - x_0)^2 + (z - z_0)^2} dx \right. \\ & \left. - \oint_C \frac{(x - x_0)^{i-n+1} (z - z_0)^{j-m+1}}{(x - x_0)^2 + (z - z_0)^2} dz \right), \end{aligned} \quad (8)$$

where \oint_C denotes counterclockwise integration along the contour of the 2D mass body (see Figure 1), which is approximated by an N_c -sided polygon. After integration along the boundary of the N_c -sided polygon, equation 8 can be rewritten as

$$\Delta g_z(x_0, z_0) = -2G \sum_{i=0}^{N_x} \sum_{j=0}^{N_z} a_{i,j} \sum_{m=0}^j C_j^m(z_0)^m \times \sum_{n=0}^i \frac{C_i^n(x_0)^n}{i+j-m-n+1} \sum_{k=1}^{N_e} E(i, j, m, n, k), \tag{9}$$

where $E(i, j, m, n, k)$ is the integral along the k th segment counter-clockwise from vertex (x_k, z_k) to vertex (x_{k+1}, z_{k+1}) (see Figure 1):

$$E(i, j, m, n, k) = \int_{z_k}^{z_{k+1}} \frac{(x-x_0)^{i-n+1}(z-z_0)^{j-m+1}}{(x-x_0)^2+(z-z_0)^2} dz - \int_{x_k}^{x_{k+1}} \frac{(x-x_0)^{i-n}(z-z_0)^{j-m+2}}{(x-x_0)^2+(z-z_0)^2} dx. \tag{10}$$

Comparing equation 9 above with equation 9 of Zhang et al. (2001), we can see that reduction from the former to the latter is done by setting $x_0 = 0$ and $z_0 = 0$.

Now following Zhou (2009b), we consider whether the k th segment is parallel to the z -axis. When the k th segment is not parallel to the z -axis, i.e., $x_k \neq x_{k+1}$, the line equation for the k th segment is

$$z = px + q, \tag{11}$$

$$p = \frac{z_{k+1} - z_k}{x_{k+1} - x_k}, \tag{12}$$

$$q = \frac{z_k x_{k+1} - z_{k+1} x_k}{x_{k+1} - x_k}. \tag{13}$$

Inserting equation 11 into equation 10 and transforming the first integral in equation 10 from z to x , then coalescing the two integrals into one, equation 10 becomes

$$E(i, j, m, n, k) = - \int_{x_k}^{x_{k+1}} \frac{(px_0 + q - z_0)(x - x_0)^{i-n}(px + q - z_0)^{j-m+1}}{(1+p^2)x^2 + 2[p(q-z_0) - x_0]x + [x_0^2 + (q-z_0)^2]} dx. \tag{14}$$

After using the binomial theorem and reorganization, it yields

$$E(i, j, m, n, k) = -(px_0 + q - z_0) \sum_{l_1=0}^{i-n} \sum_{l_2=0}^{j-m+1} C_{i-n}^{l_1} C_{j-m+1}^{l_2} \times p^{j-m-l_2+1} (-x_0)^{l_1} (q-z_0)^{l_2} \times I_{i+j-m-n-l_1-l_2+1}, \tag{15}$$

where, when $\ell = i + j - m - n - l_1 - l_2 + 1$,

$$I_\ell = \int_{x_k}^{x_{k+1}} \frac{x^\ell}{cx^2 + bx + a} dx, \tag{16}$$

with $a = x_0^2 + (q - z_0)^2$, $b = 2[p(q - z_0) - x_0]$, and $c = 1 + p^2$.

Let's define $Q = 4ac - b^2 = 4(px_0 + q - z_0)^2 \geq 0$. Two cases need to be considered: $Q = 0$ and $Q > 0$. For $Q = 0$, i.e., $px_0 + q - z_0 = 0$, equation 15 becomes

$$E(i, j, m, n, k) = 0. \tag{17}$$

With $Q > 0$, the integral in equation 16 is recursive because

$$\int \frac{x^n}{a + bx + cx^2} dx = \frac{x^{n-1}}{(n-1)c} - \frac{b}{c} \int \frac{x^{n-1}}{a + bx + cx^2} dx - \frac{a}{c} \int \frac{x^{n-2}}{a + bx + cx^2} dx$$

(Beyer, 1984). The series of the recursive integrals is given as

$$I_0 = \frac{1}{|px_0 + q - z_0|} \left(\tan^{-1} \frac{(1+p^2)x_{k+1} + p(q-z_0) - x_0}{|px_0 + q - z_0|} - \tan^{-1} \frac{(1+p^2)x_k + p(q-z_0) - x_0}{|px_0 + q - z_0|} \right), \tag{18}$$

$$I_1 = \frac{1}{(1+p^2)} \ln \frac{r_{k+1}}{r_k} - \frac{p(q-z_0) - x_0}{1+p^2} I_0, \tag{19}$$

$$I_\ell = \frac{1}{(\ell-1)(1+p^2)} (x_{k+1}^{\ell-1} - x_k^{\ell-1}) - \frac{2[p(q-z_0) - x_0]}{1+p^2} I_{\ell-1} - \frac{(q-z_0)^2 + x_0^2}{1+p^2} I_{\ell-2}, \tag{20}$$

where

$$r_{k+1} = \sqrt{(x_{k+1} - x_0)^2 + (z_{k+1} - z_0)^2}$$

and

$$r_k = \sqrt{(x_k - x_0)^2 + (z_k - z_0)^2}$$

(see Figure 1).

When the k th segment is parallel to the z -axis, i.e., $x_k = x_{k+1}$, equation 10 for the $E(i, j, m, n, k)$ function is given by

$$E(i, j, m, n, k) = (x_k - x_0)^{i-n+1} K_{j-m+1}, \tag{21}$$

where, when $\ell = j - m + 1$, K_{j-m+1} is given by

$$K_\ell = \int_{z_k}^{z_{k+1}} \frac{(z-z_0)^\ell}{(x_k - x_0)^2 + (z-z_0)^2} dz. \tag{22}$$

From equation 3, for $j = 0$, I have $m = 0$; for $j \geq 1$, I have $m = 0, 1, \dots, j$. The range of the value of the index ℓ of K_ℓ is from zero to $j + 1$. Without loss of generality, the series of the recursive integrals for K_ℓ can be found by setting $m = 0$. For $j = 0$ with $\ell = 1$,

$$K_1 = \ln\left(\frac{r_{k+1}}{r_k}\right). \quad (23)$$

For $j = 1$ with $\ell = 2$,

$$K_2 = (z_{k+1} - z_k) - |x_k - x_0| \left(\tan^{-1}\left(\frac{z_{k+1} - z_0}{|x_k - x_0|}\right) - \tan^{-1}\left(\frac{z_k - z_0}{|x_k - x_0|}\right) \right). \quad (24)$$

Using equation 24 of Zhang et al. (2001) for $\ell \geq 2$, the recursive integral equation 22 becomes

$$K_\ell = \frac{1}{\ell - 1} [(z_{k+1} - z_0)^{\ell-1} - (z_k - z_0)^{\ell-1}] - (x_k - x_0)^2 K_{\ell-2}. \quad (25)$$

Now equations 9, 15, 17–21, and 23–25 form a complete set of analytic equations for the gravity-anomaly calculation at any point $P(x_0, z_0)$ in the x - z -plane outside the mass body based on the ST method.

Let's consider the analytic solution obtained by the CT method. Assume the observation point is (x_0, z_0) in the original survey coordinate system (x, z) from which the solution at the origin has been formalized (Zhang et al., 2001; Zhou, 2009b). To make the observation point the origin of the new coordinate system (x', z') , we perform a coordinate transformation:

$$x' = x - x_0, \quad (26)$$

$$z' = z - z_0. \quad (27)$$

Under such a coordinate transformation, the density contrast is expressed as a polynomial function in the new coordinate system, i.e.,

$$\sigma = \sum_{i=0}^{N_x} \sum_{j=0}^{N_z} a_{ij} x'^i z'^j = \sum_{i=0}^{N_x} \sum_{j=0}^{N_z} a'_{ij} (x')^i (z')^j, \quad (28)$$

where the new coefficient a'_{ij} is given as

$$a'_{ij} = \sum_{m=i}^{N_x} \sum_{n=j}^{N_z} a_{mn} C_m^i C_n^j x_0^{m-i} z_0^{n-j}. \quad (29)$$

Correspondingly, the geometry of the mass source in the new coordinate system is obtained through equations 26 and 27. Then the solution at the origin of the new coordinate system (Zhou, 2009b) is expressed in the original survey coordinate system so that the forward modeling for a survey at any number of stations can be automated, i.e.,

$$\Delta g(x_0, z_0) = -2G \sum_{i=0}^{N_x} \sum_{j=0}^{N_z} \frac{a'_{ij}}{i+j+1} \sum_{k=1}^{N_e} E(i, j, k). \quad (30)$$

When the k th segment is not parallel to the z -axis, i.e., $x_k \neq x_{k+1}$, then $E(i, j, k)$ in equation 30 is given by

$$E(i, j, k)$$

$$= \begin{cases} 0, & \text{for } q' = 0, \\ -\sum_{l=0}^{j+1} C_{j+1}^l p^{j-l+1} (q')^{l+1} I'_{i+j-l+1}, & \text{for } q' \neq 0, \end{cases} \quad (31)$$

$$q' = \frac{z'_k x'_{k+1} - z'_{k+1} x'_k}{x'_{k+1} - x'_k} = q + px_0 - z_0, \quad (32)$$

where p and q are given by equations 12 and 13. The integrals $I'_{i+j-l+1}$ in equation 31 are

$$I'_0 = I_0, \quad (33)$$

$$I'_1 = I_1 - x_0 I_0, \quad (34)$$

$$I'_\ell = \frac{1}{(\ell-1)(1+p^2)} [(x_{k+1} - x_0)^{\ell-1} - (x_k - x_0)^{\ell-1}] - \frac{2pq'}{1+p^2} I'_{\ell-1} - \frac{(q')^2}{1+p^2} I'_{\ell-2}, \quad (\ell > 1), \quad (35)$$

where I_0 and I_1 are given by equations 18 and 19.

When the k th segment is parallel to the z -axis, i.e., $x_k = x_{k+1}$, then $E(i, j, k)$ in equation 30 is given by

$$E(i, j, k) = (x_k - x_0)^{i+1} K_{j+1},$$

where K_ℓ ($\ell = j+1 = 1, 2, 3, \dots$) are given by equations 23–25. Now equations 29–35 form a complete set of analytic equations for the gravity-anomaly calculation at any point $P(x_0, z_0)$ in the x - z -plane outside the mass body that are obtained from the CT method based on the solution at the origin (Zhou, 2009b).

SINGULARITY AND NUMERICAL INSTABILITY

When the observation point is coincident with the vertices of the geometry of the mass body, singularity occurs, resulting in calculation errors. When the k th segment is not parallel to the z -axis, i.e., $x_k \neq x_{k+1}$, singularity occurs in the argument of the natural logarithm function in equation 19 that is used for the analytical methods obtained by the ST and CT methods (see equations 19 and 34). However, singularity will not appear in the argument of the arctangent function in equation 18 because when $px_0 + q - z_0 = 0$, then $E(i, j, m, n, k)$ is given by equation 15. When the k th segment is parallel to the z -axis, i.e., $x_k = x_{k+1}$, and the observation point is coincident with the vertices of the geometry of the mass body, singularity occurs in the arguments of the arctangent and natural logarithm functions in equations 23 and 24 that are used for both analytical solutions.

In either case, the arctangent or natural logarithm function is a multivariate function. There is no l'Hopital's rule for finding the limit of a multivariate function, so the limit is discovered by allowing the observation point (x_0, z_0) to approach the vertex (x_k, z_k) or (x_{k+1}, z_{k+1}) along any curve that passes through (x_k, z_k) or (x_{k+1}, z_{k+1}) . Often, it is easier to show that a limit does not exist by demonstrating that the limit has different values, depending on the curve used. For the natural logarithm function in equations 19 and 23, limit does not exist as the observation point (x_0, z_0) approaches the vertex (x_k, z_k) or (x_{k+1}, z_{k+1}) .

For the arctangent function in equation 24, consider the case when the observation point (x_0, z_0) approaches the vertex (x_k, z_k) . Assume the approach is along the curves $z_0 - z_k = S(x_0 - x_k)$ through the vertex (x_k, z_k) , where S is the slope,

$$\lim_{(x_0, z_0) \rightarrow (x_k, z_k)} \left(\frac{z_k - z_0}{|x_k - x_0|} \right) = - \lim_{(x_0, z_0) \rightarrow (x_k, z_k)} \left(\frac{S(x_0 - x_k)}{|x_0 - x_k|} \right) = -S \cdot \text{sgn}(x_0 - x_k). \quad (36)$$

Here, the sign function $\text{sgn}(x)$ is defined as

$$\text{sgn}(x) = \begin{cases} -1 & \text{for } x < 0 \\ +1 & \text{for } x > 0 \end{cases}.$$

The limit of $(z_k - z_0)/|x_k - x_0|$ is dependent on S as observation point (x_0, z_0) approaches the vertex. This means the limit of $(z_k - z_0)/|x_k - x_0|$ does not exist, so neither does $\tan^{-1}((z_k - z_0)/|x_k - x_0|)$.

When gravity stations are at a vertex of the mass polygon, singularity occurs because the log and arctangent functions are undefined. A convenient and practical way to remove the singularity is to use the exclusive infinitesimal sphere method to avoid divergence in numerical computation (Zhou, 2009c) because the values on the surface of the exclusion are very similar and the anomaly is continuous across the surface. Although the logarithm function passes through an infinite singularity, it has a multiplier that tends to zero, rendering the overall value finite. The same goes for the arctangent function. The gravity anomaly at the vertex is thus defined. Generally, the radius of the exclusive infinitesimal sphere can be specified as $\varepsilon = \mu R_m$, where μ is a dimensionless, infinitely smaller number and R_m is the maximum size of the mass body. In the following discussion, an exclusive infinitesimal circle with a radius of 10^{-15} m around the singular point is used to calculate the arctangent and natural logarithm functions.

Numerical stability is a desired property of any algorithm. However, numerical calculation is often contaminated by numerical instability; small errors from round-off or truncation can be magnified, leading to large errors — even though the mathematics in the algorithm development are perfect. To evaluate the stability of the analytic algorithm developed above, consider a square object $\{[x, z]: -1 \leq x, z \leq +1\}$ with density contrast

$$\sigma(x, z) = x^3 z^3, \quad (37)$$

where $\sigma(x, z)$ is in g/cm^3 and where x and z are in meters (units are consistent for σ , x , and z unless otherwise noted). For such an object, the total mass contrast is zero: $\Delta m = \int_{-1}^{+1} dx \int_{-1}^{+1} dz x^3 z^3 = 0$. The parts of the object in the first and third quadrants have positive mass density contrast, and the parts in the second and fourth quadrants have negative mass density contrast. This means (1) the gravity anomaly at points close to the object along line $z = x$ in the first quadrant should have positive gravity anomaly and (2) the gravity anomaly at an observation point far from the object should approach zero as the distance from the object increases. From equation 2, the gravity anomaly at any observation point outside the object is

$$\Delta g_z(x_0, z_0) = -2G \int_{-1}^{+1} \int_{-1}^{+1} \frac{x^3 z^3 (z - z_0)}{(x - x_0)^2 + (z - z_0)^2} dx dz, \quad (38)$$

where the negative sign is from the opposite direction of gravity to the direction of z -axis in the coordinate setup.

Three methods are used to calculate the gravity anomaly at points along line $z = x$ at a length interval of $\sqrt{2}$ from point (2,2) to point (100,100): the analytic algorithms based on the ST and the CT methods and the direct numerical integration of equation 38 using the Simpson algorithm with variable steps. The computation is performed on a Dell Optiplex GX 620 desktop computer. Test runs show that all methods work very well for points close to the object. Thus, the gravity anomaly at point (2,2) is used for intercalibration among the three algorithms; all methods produce the gravity anomaly at point (2,2) with a difference of no more than 1.5×10^{-12} mGal. The difference between the ST and CT analytic algorithms at point (2,2) is 1.6×10^{-16} mGal.

Figure 2a compares the gravity anomaly versus the x -coordinate of the observation points calculated by the three methods. Instability does not occur for the numerical integration using the Simpson algorithm within the calculation range ($x_0 \in [2, 100]$). Figure 2b shows the logarithm of relative error to base 10 versus the x -coordinate of the observation points, where the result at each station calculated using the numerical integration is used as the exact value for the relative error calculation. When the logarithm of the relative error reaches zero, we have a 100% relative error. For this example, the 100% relative error occurs at $x_0 = 33$ m (16.5 target diameters) for the ST method and at $x_0 = 32$ m (16 target diameters) for the CT method. To achieve a relative error of 10^{-4} , we need to be within 5.5 target diameters for both the analytic methods.

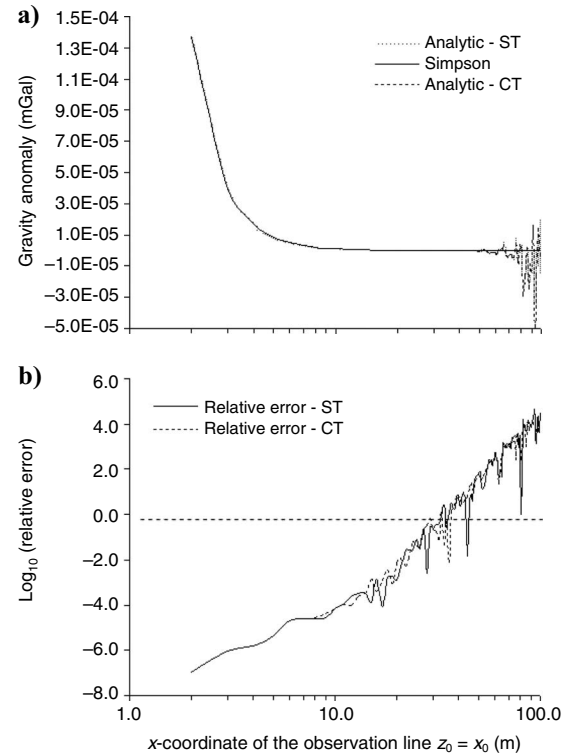


Figure 2. (a) Gravity anomaly calculated by the analytic solutions obtained using the ST and CT methods and numerical integration using the Simpson algorithm for a square object $\{[x, z]: -1 \leq x, z \leq +1\}$ with density contrast $\sigma(x, z) = x^3 z^3$. (b) Logarithm of the relative error versus the x -coordinate of the observation line for the ST and CT algorithms.

The target distance within which the relative error is within 100% is referred to as the range of numerical stability of the algorithm. The magnitude of fluctuation increases with increasing target distance when the relative error reaches 100% (Figure 2a) for both analytic methods. The maximum difference between the ST and CT methods within the calculation range ($x_0 \in [2, 100]$) is 2.1×10^{-5} mGal, occurring at $x_0 = 93$ m — well beyond the range of numerical stability of both algorithms. Within the range of numerical stability of 16 target diameters, the maximum difference between ST and CT methods is less than 1.6×10^{-8} mGal. The difference between the ST and Simpson methods (absolute value) exceeds 1.0×10^{-7} mGal when $x_0 > 42$ m (21 times the diameter of the target); the difference between the CT and Simpson methods exceeds 1.0×10^{-7} mGal when $x_0 > 39$ m (19.5 times the diameter of the target).

The actual values above are problem-dependent. These comparisons and Figure 2 show that results from the ST and CT methods are very similar. Also, singularity that occurs in the arctangent and natural logarithm functions in equations 19, 23, and 24 is the same for the ST and CT methods. Thus, in the following discussion, only results from the ST method are shown.

Further tests between the ST and Simpson methods are performed for density-contrast functions such as $\sigma(x, z) = xz, xz^2, x^2z,$ and x^5z^5 so that all distributions result in zero total mass contrast. Instability occurs for all distributions. Relative error reaches 100% at shorter distances from the source for higher-order distributions. For instance, the relative error exceeds 100% at about $x_0 = 374$ m (187 times the diameter) for lower-order term xz , but for the higher-order term x^5z^5 , the relative error reaches 100% at about $x_0 = 10$ m (five times the diameter). For distributions xz^2 and x^2z , the relative error reaches 100% at about $x_0 = 355$ m (175.5 times the diameter).

Similar tests are performed for density-contrast functions such as $\sigma(x, z) = x, z, x^2, z^2, x^2z^2,$ and x^4z^4 ; all distributions result in nonzero total mass contrast. For these distributions, the distance from the source at which the relative error reaches 100% is 8100 m for $\sigma(x, z) = x$ or z , 6930 m for $\sigma(x, z) = x^2$ or z^2 , 370 m for $\sigma(x, z) = x^2z^2$, and 31 m for $\sigma(x, z) = x^4z^4$. These tested density-contrast functions and the corresponding ranges of numerical stability (relative error $\leq 100\%$) are summarized in Table 1; we can see that terms of nonzero total mass contrast of higher order have similar ranges of

Table 1. Ranges of numerical stability for the ST analytic algorithm for various density-contrast distributions for a square object $\{[x, z]: -1 \leq x, z \leq +1\}$. The diameter of the target is approximated as 2 m.

$\sigma(x, z)$	Range of stability (unit: diameter of target)	Total mass contrast
x or z	$x_0 \leq 4050$	Zero
xz	$x_0 \leq 187$	Zero
x^2 or z^2	$x_0 \leq 3465$	Nonzero
xz^2 or x^2z	$x_0 \leq 177.5$	Zero
x^2z^2	$x_0 \leq 185$	Nonzero
x^3z^3	$x_0 \leq 16.5$	Zero
x^4z^4	$x_0 \leq 15.5$	Nonzero
x^5z^5	$x_0 \leq 5$	Zero
Equation 41	$x_0 > 5000$	Nonzero
Equation 42	$x_0 > 5000$	Nonzero

numerical stability. For instance, x^2z^2 (nonzero mass contrast) has a similar range of numerical stability as $xz, xz^2,$ and x^2z (zero mass contrast); likewise, x^4z^4 has a similar range of stability as x^3z^3 .

To test the stability of the density-contrast function of multiple terms, I use the two density-contrast functions (equations 41 and 42) for the same square object, $\{[x, z]: -1 \leq x, z \leq +1\}$. Figure 3a shows the gravity anomaly versus the x -coordinate of the observation points along line $z = x$ in the first quadrant, using the analytic method for the two density-contrast distributions. Figure 3b shows the logarithm of the relative error to base 10, where the exact value at each station is calculated using the numerical integration (Simpson algorithm) for each density-contrast distribution. The gravity anomaly at point (2, 2) is intercalibrated between the analytic method and the numerical integration method with a difference of no more than 3.6×10^{-12} mGal for equation 41 and no more than 1.1×10^{-11} mGal for equation 42. For the calculated range of x_0 (up to 5000 times the diameter of the target), relative error caused by numerical instability does not reach 100%. The range of stability exceeds 5000 times the diameter of the target for both cases (Table 1). For the tested range between $x_0 = 2$ m, $x_0 = 10,000$ m, the maximum absolute difference in the calculated gravity anomaly between the analytic and numerical methods is 1.8×10^{-11} mGal for equation 41 and 1.7×10^{-11} mGal for equation 42. For both cases, instability occurs with relative error varying in the range of 10^{-7} to 10^{-14} , which is obviously negligible.

VERIFICATION OF ANALYTIC SOLUTION

To validate the analytic solutions obtained for the gravity anomaly at any point along the x -axis for an irregular mass body with poly-

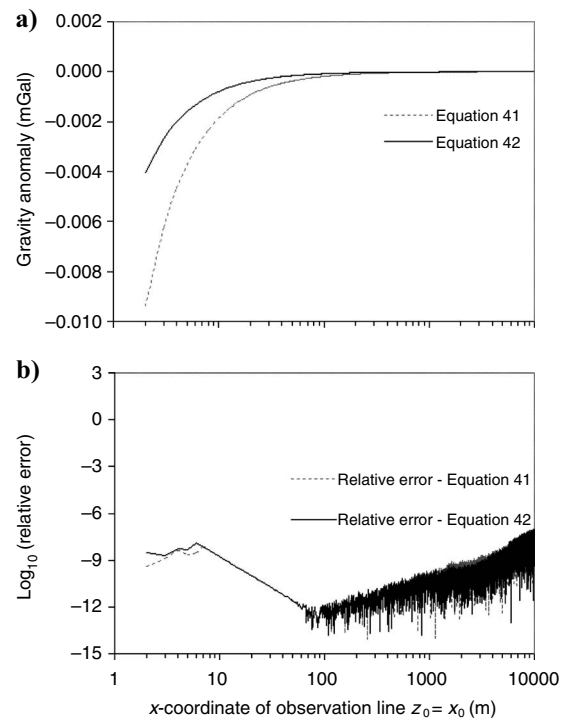


Figure 3. (a) Gravity anomaly calculated by the ST analytic method for a square object $\{[x, z]: -1 \leq x, z \leq +1\}$ with density contrast functions given by equations 41 and 42. (b) Logarithm of the relative error versus the x -coordinate of the observation line. Even when $x_0 = 10,000$ m (5000 times the diameter of the target), the relative error caused by numerical instability does not reach 100%.

mial density contrast function, I compare the results from the above analytic solution with those of the line integral (LI) method (Zhou, 2008; 2009a) and results by Martín-Atienza and García-Abdeslem (1999). For this purpose, I consider three cases of the density contrast function: (1) a polynomial function of only the horizontal direction x , (2) a polynomial function of only the vertical direction z , and (3) a polynomial function of x and z . All calculations in the following examples are performed at points near the targets and thus within the range of numerical stability.

Cases with density contrast as a polynomial function of horizontal direction

For cases with the density contrast depending only on the horizontal position $N_z = 0$, equation 1 becomes $\sigma(x) = \sum_{i=0}^{N_x} a_{i0}x^i$. Figure 4 depicts a case studied by Martín-Atienza and García-Abdeslem (1999) and Zhou (2009a). Figure 4a shows the geometry of a mass body with density contrast dependent only on horizontal position x :

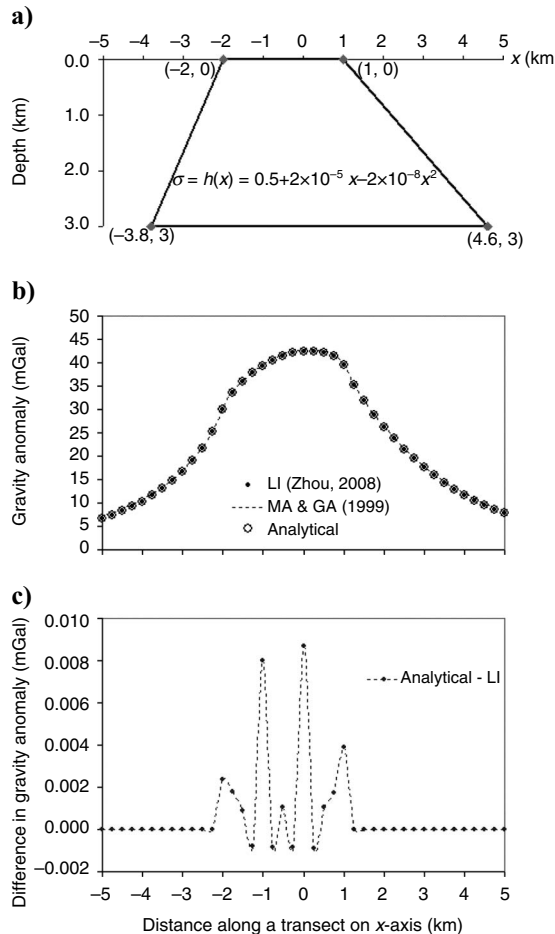


Figure 4. (a) Simple geometry of a 2D mass body, with density contrast a polynomial function of only horizontal position x : $\sigma(x) = 0.5 + 2 \times 10^{-5}x - 2 \times 10^{-8}x^2$. (b) The gravity anomalies along a transect on the x -axis ($z_0 = 0$) calculated using the ST analytic method, the LI with logarithmic kernel (Zhou, 2009a), and the results by Martín-Atienza and García-Abdeslem (MA & GA) (1999). (c) The difference in calculated gravity anomalies using the ST analytical method and the LI method (Zhou, 2009a).

$$\sigma = h(x) = 0.5 + 2 \times 10^{-5}x - 2 \times 10^{-8}x^2. \quad (39)$$

Figure 4b compares the gravity anomaly calculated along transect on the x -axis ($z_0 = 0$) using the analytic method, the LI method (Zhou, 2009a), and results by Martín-Atienza and García-Abdeslem (1999). The results from the LI method were calculated with the number of nodes for Gaussian quadrature $k = 20$ at 41 stations. To avoid divergence from singularity when the observation point is coincident with vertices of the polygonal mass body during calculation, an infinitesimal circle of radius of 10^{-15} m is excluded from calculation at singularity points. From Figure 4b, we see that the three methods agree very well.

Figure 4c shows the difference between the seminumerical calculation using the LI method (Zhou, 2009a) and the analytic method. For stations away from the mass source ($x < -2$ km and $x > 1$ km), the difference between the LI method and the analytic method is smaller than 4.2×10^{-7} mGal. The maximum difference between the two methods is 0.0087 mGal, occurring at the origin ($x = 0$ km). The difference results from the singularity in both methods. When the calculation point locates at the vertices of the mass polygon, singularity occurs in both methods; when the calculation point locates at the edges but between vertices, singularity occurs in the LI method. The calculation is performed at points near the mass source, so no numerical instability occurs.

Cases with density contrast as a polynomial function of vertical direction

For cases with the density contrast depending only on the vertical position $N_x = 0$, equation 1 becomes $\sigma(z) = \sum_{j=0}^{N_z} a_{0j}z^j$. Figure 5 shows a case studied by Zhou (2008) using LI with arctangent kernel and with algebraic kernel. Figure 5a shows the geometry of a mass body with density contrast dependent only on vertical position z :

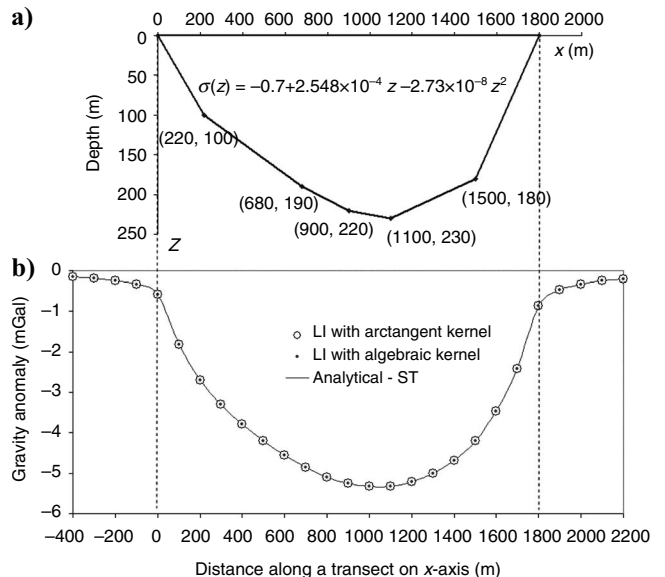


Figure 5. (a) Polygon contour of a 2D mass. The model represents the 2D cross section of an elongated sediment valley, with sedimentary density contrast a polynomial function of vertical depth only: $\sigma(z) = -0.7 + 2.548 \times 10^{-4}z - 2.73 \times 10^{-8}z^2$ g/cm³. (b) Gravity anomalies calculated using the LIs with arctangent kernel and algebraic kernel (Zhou, 2008) compared with those calculated using the ST analytic method.

$$\sigma = v(z) = -0.7 + 2.548 \times 10^{-4}z - 2.73 \times 10^{-8}z^2, \quad (40)$$

where $\sigma = v(z)$ is in g/cm^3 , and z is in m . Figure 5b compares the gravity anomaly calculated along transect on the x -axis ($z_0 = 0$) using the analytic method, LI with arctangent kernel, and LI with algebraic kernel (Zhou, 2008). The results from the LI methods were calculated with the number of nodes for Gaussian quadrature $k = 30$ at 27 stations.

From Figure 5b, we can see that the three methods agree very well. The maximum difference between the LI methods (LIs with both arctangent kernel and with algebraic kernel) and analytic method is 1.24×10^{-14} mGal occurring at the station of $x = 1200$ m. Excellent agreement is observed even at stations within the source region ($0 < x < 1800$ m) when the density contrast depends only on depth.

Cases with density contrast as a polynomial function of horizontal and vertical positions

For more general cases with density contrast varying with the horizontal and vertical positions, I consider the following case studied by Martín-Atienza and García-Abdeslem (1999) and Zhou (2009a).

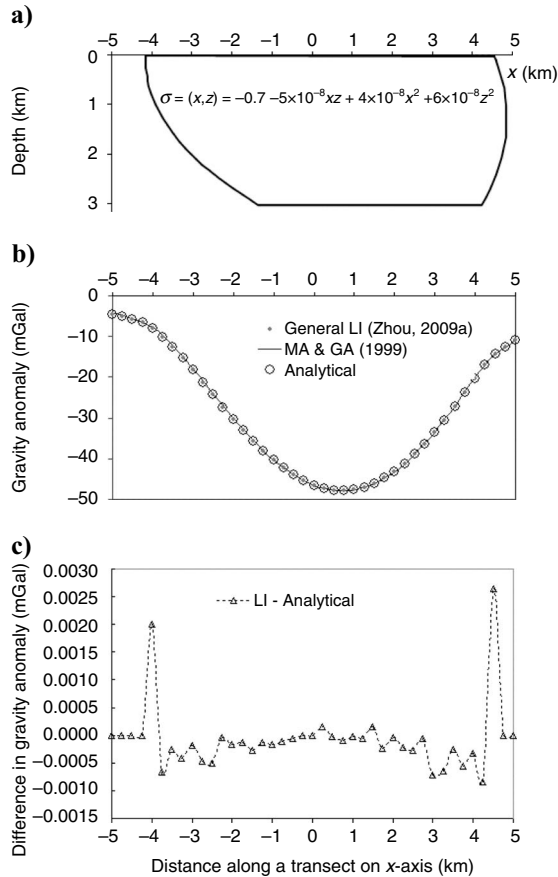


Figure 6. (a) Geometry of an irregular mass body, representing folded and overturned strata in a sedimentary basin. The density contrast is $\sigma(x,z) = -0.7 - 5 \times 10^{-8}xz + 4 \times 10^{-8}x^2 + 6 \times 10^{-8}z^2$. (b) The gravity anomalies calculated using the ST analytic method, the LI with logarithmic kernel (Zhou, 2009a), and the results by Martín-Atienza and García-Abdeslem (MA & GA) (1999). (c) The difference in calculated gravity anomalies using the analytic and the LI methods (Zhou, 2009a).

Figure 6a shows the geometry of an irregular mass body, representing folded and overturned strata in a sedimentary basin. The density contrast varies as a polynomial function in the horizontal and vertical directions:

$$\sigma(x,z) = -0.7 - 5 \times 10^{-8}xz + 4 \times 10^{-8}x^2 + 6 \times 10^{-8}z^2. \quad (41)$$

For this density-contrast model, N_x and N_z are two and the coefficients are $a_{00} = -0.7$, $a_{02} = 6 \times 10^{-8}$, $a_{11} = -5 \times 10^{-8}$, $a_{20} = 4 \times 10^{-8}$, and $a_{01} = a_{10} = a_{12} = a_{21} = a_{22} = 0$. The boundary of the 2D mass is approximated as a 26-sided polygon, and the gravity anomaly was calculated at 41 stations.

Figure 6b compares the gravity anomaly calculated along transect on the x -axis ($z_0 = 0$) using the seminumerical LI method (Zhou, 2009a), results obtained by Martín-Atienza and García-Abdeslem (1999), and the analytic method. The results using the analytic method agree very well with the general LI method (Zhou, 2009a) and those by Martín-Atienza and García-Abdeslem (1999).

Figure 6c shows the difference between the general LI method and the analytic method. The maximum difference between the two methods is 0.0026 mGal, occurring at the station of $x = 4.5$ km. Similar to the comparison for the case with density contrast as a polynomial function of the horizontal direction, the main difference occurs in the source region ($-4 < x < 4.5$ km). For stations away from the mass source ($x < -4$ km and $x > 4.5$ km), the difference between the methods is very small ($< 3.78 \times 10^{-8}$ mGal).

To test if the analytic method works well in calculating the gravity anomaly on an undulating surface, the case of Figure 8 of Martín-Atienza and García-Abdeslem (1999) is used because the calculated gravity anomaly data provided by García-Abdeslem are available for comparison. Figure 7a shows the contour of the mass body that is bounded by $-5000 \leq x \leq +5000$ in the x -direction; $z_1(x) \leq z \leq z_2(x)$, where $z_1(x) = -100 + 0.03x + 10^{-6}x^2 + 5 \times 10^{-9}x^3$ and $z_2(x) = 3000 - 0.02x - 10^{-6}x^2 - 7 \times 10^{-9}x^3$. The density contrast is

$$\sigma(x,z) = -0.3 - 5 \times 10^{-5}x + 9 \times 10^{-5}z - 1.0 \times 10^{-8}x^2 + 1.0 \times 10^{-8}z^2. \quad (42)$$

The contour of the mass body is divided into 200 segments. Gravity anomaly is calculated on 100 stations on the top curve $z_1(x)$.

Figure 7b shows the comparison of the gravity anomaly calculated along the curve $z_1(x)$ using the seminumerical LI method (Zhou, 2009a), results by Martín-Atienza and García-Abdeslem (1999), and the present analytic method. The results using the analytic method agree very well with the general LI method (Zhou, 2009a) and those by Martín-Atienza and García-Abdeslem (1999) on the undulated curve.

Figure 5c shows the difference between the analytic method and the general LI method and between the analytic method and the results by Martín-Atienza and García-Abdeslem (1999). The maximum difference between the analytic method and the general LI method is 1.63×10^{-4} mGal. The maximum difference between the analytic method and the results calculated by Martín-Atienza and García-Abdeslem (1999) is 0.0576 mGal. The results from the analytic and LI methods are very close.

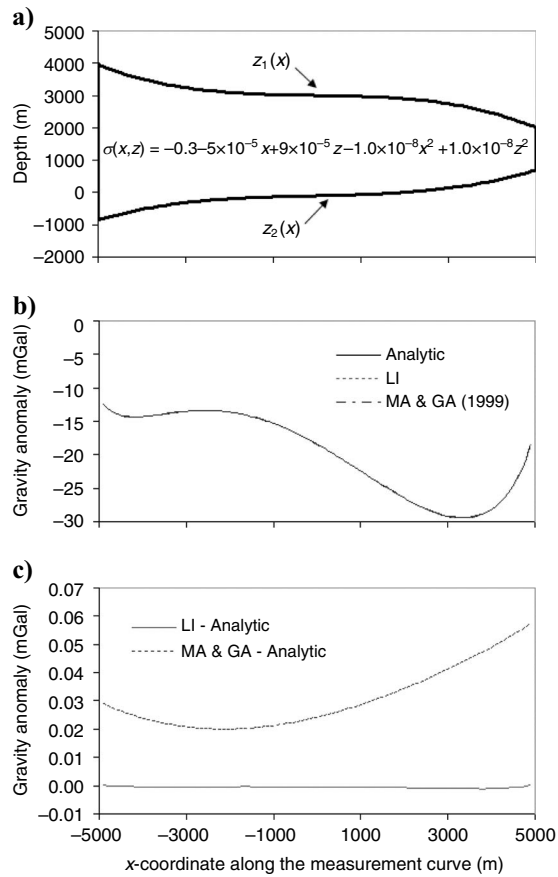


Figure 7. (a) Geometry of an irregular mass body, representing uneven top surface where calculation is made. Density contrast is $\sigma(x,z) = -0.3 - 5 \times 10^{-5}x + 9 \times 10^{-5}z - 1.0 \times 10^{-8}x^2 + 1.0 \times 10^{-8}z^2$. (b) Gravity anomalies calculated using the ST analytic method, the LI (Zhou, 2009a), and the results by Martín-Atienza and García-Abdeslem (1999). (c) Difference in calculated gravity anomalies between the ST analytic and LI methods (Zhou, 2009a) and between the ST analytic method and Martín-Atienza and García-Abdeslem (1999).

CONCLUSIONS

For the density contrast of an irregular 2D mass body approximated as a polynomial function, which is usually a least-squares fitting to the density logging data, we expand the closed-form solution at the origin to any station by reformulating the solution, while keeping the density-contrast profile and the geometry intact, or transforming the coordinate system. The closed-form solution for any surface station is then programmable to calculate gravity anomaly, rather than by dividing the source mass into columns and using a 1D vertical density-contrast model to calculate the gravity at any station. The source codes of some computer programs used to generate relevant figures in this paper are available upon request.

Singularity occurs in the arctangent and natural logarithm functions in the analytic solution when the observation points are coincident with the vertices of the polygonal mass body. An infinitesimal

circle around each singular point is excluded from calculation to avoid divergence in numerical calculation. Case studies show that numerical instability occurs in the analytical method but not in direct numerical integration using the Simpson method. The range of numerical stability is defined as the distance from the source mass center to the observation point when the relative error reaches 100%. It is dependent on specific questions but generally decreases for terms of higher order in the polynomial density-contrast function. Compared with single terms in the polynomial function of the density contrast, instability seems to be suppressed for a polynomial of multiple terms owing to cancellation of errors from individual terms, resulting in negligible errors within a range of 5000 times the size (diameter) of the target.

The complete set of analytic equations was tested through comparison with other numerical or seminumerical methods. The analytic method agrees very well with other methods when the observation points are within the range of numerical stability, which is usually the case for the ground gravity survey. This indicates that within the range of numerical stability, my closed-form solution is accurate and can be used for irregular 2D mass bodies when the density contrast can be approximated as a polynomial function in horizontal and/or vertical positions. However, caution should be exercised in modeling or interpreting the gravity-survey data using the analytic methods when the target distance is outside the range of numerical stability. For distant targets, a switch from analytical method to numerical integration may be necessary for accuracy.

ACKNOWLEDGMENTS

The critiques and helpful comments and suggestions by reviewers Juan García Abdeslem, Horst Holstein, Alton K. Schultz, associate editor Xiong Li, and an anonymous reviewer are very much appreciated. I also thank Juan García Abdeslem for providing data so that quantitative comparison in Figure 7 is possible. The formula for the polynomial coefficient in the transformed coordinate system was provided by Horst Holstein; the discussion on the numerical stability was inspired by a discussion with him.

REFERENCES

- Beyer, W. H., 1984, CRC standard mathematical tables, 27th ed.: CRC Press, 244–245.
- Martín-Atienza, B., and J. García-Abdeslem, 1999, 2-D gravity modeling with analytically defined geometry and quadratic polynomial density functions: *Geophysics*, **64**, 1730–1734.
- Zhang, J., B. Zhong, X. Zhou, and Y. Dai, 2001, Gravity anomalies of 2-D bodies with variable density contrast: *Geophysics*, **66**, 809–813.
- Zhou, X., 2008, 2D vector gravity potential and general line integrals for gravity anomaly due to 2D masses of depth-dependent density contrast: *Geophysics*, **73**, no. 6, I43–I50.
- , 2009a, General line integrals for gravity anomalies of irregular 2D masses with horizontally and vertically dependent density contrast: *Geophysics*, **74**, no. 2, I1–I7.
- , 2009b, Discussion on “Gravity anomalies of 2D bodies with variable density contrast” (Jianzhong Zhang, Benshan Zhong, Xixiang Zhou, and Yun Dai, 2001, *Geophysics*, **66**, no. 3, 809–813): *Geophysics*, **74**, no. 4, X3–X4.
- , 2009c, 3D vector gravity potential and line integrals for the gravity anomaly of a rectangular prism with 3D variable density contrast: *Geophysics*, **74**, no. 6, I43–I53.